

Statistical and dynamical parts of the cumulants of conserved charges in relativistic heavy ion collisions

Xue Pan,^{1,*} Fan Zhang,¹ Zhiming Li,¹ Lizhu Chen,² Mingmei Xu,¹ and Yuanfang Wu^{1,†}

¹*Key Laboratory of Quark and Lepton Physics (MOE) and Institute of Particle Physics, Central China Normal University, Wuhan 430079, China*

²*School of Physics and Optoelectronic Engineering, Nanjing University of Information Science and Technology, Nanjing 210044, China*

The Poisson-liked statistical fluctuations, which are caused by the finite number of produced particles, are firstly estimated for the cumulants of conserved charges, i.e., the cumulants of net-baryon, net-electric charge, and net-strangeness. They turn out to be the same as those baselines derived from Hadron Resonance Gas (HRG) model. The incident energy and centrality dependence of net-proton cumulants at RHIC energies are demonstrated to be mainly caused by statistical fluctuations. Subtracting the statistical fluctuations, the dynamical net- and total-proton kurtosis from two versions of the AMPT model and the UrQMD model at RHIC beam energy scan (BES) energies are presented. It is found that the observed sign change of net-proton kurtosis can not be reproduced by these three transport models. There is no significant difference between net- and total-proton kurtosis in model calculations, in contrary to the data at RHIC/BES energies.

PACS numbers: 25.75.Nq, 25.75.Gz

I. INTRODUCTION

The cumulants of conserved charges are suggested as good probes of QCD phase boundary. They are experimentally accessible and theoretically calculable.

At finite temperature and baryon chemical potential, effective chiral models [1] and some lattice QCD calculations [2, 3] have predicted the existence of the QCD critical point (CP). Since the higher order cumulants of conserved charges are more sensitive to the correlation length, they are suggested as critical related measurements in heavy ion collisions [4–8].

At vanishing chemical potential, the lattice QCD calculations at physical quark masses have shown that the chiral crossover transition appears as the remnants of the second order phase transition belonging to the $O(4)$ universality class [9, 10]. This makes it possible to explore the temperature of QCD phase transition by the associated singularities of the higher order cumulants of conserved charges [11–14].

Moreover, recent calculations of lattice QCD indicate that the freeze-out conditions in heavy ion collisions can be reliably determined by the ratios of the first three order cumulants of net-electric charge [15]. So the measurements of the cumulants of conserved charges are crucial in locating the QCD phase boundary.

Before understanding the physics of measured cumulants, we should be clear on the contributions of various non-critical effects, such as global conservation laws in a subsystem [16], initial size fluctuations [17] and experimental acceptance cuts [17, 18]. In the paper, we will focus on the contributions of Poisson-liked statistical fluctuation, which is caused by the finite number of produced particles [19–21].

For an ideal thermodynamic system, the number of particles is infinitely large. The statistical fluctuations are small and negligible in comparison to the critical one. However, for the heavy ion collisions at RHIC, the number of produced particles is not infinitely large. For example, at the top of RHIC energies, the mean of net-proton is less than 10 [22]. Therefore, the statistical fluctuations are not negligible.

The calculations of a multiphase transport (AMPT) model [23] have shown that the statistical fluctuations dominate the behavior of the net-proton cumulants at RHIC energies [24]. Here, we further compare the experimentally measured net-proton cumulants with corresponding statistical fluctuations. It shows clearly how the statistical fluctuations dominate the behaviour of net-proton cumulants at nine centralities and three RHIC energies.

Subtracting the Poisson-liked statistical fluctuations, the dynamical net-proton cumulants are recommended [8, 24]. From the calculation of non-linear σ model [8] and the arguments of universality near the critical point [25], the dynamical net-proton kurtosis is negative when the critical point is approached from high temperature side.

Corresponding experimental measurements at RHIC/BES have observed expected sign change, i.e., the dynamical net-proton kurtosis varies from negative to positive when centrality varies from central to peripheral collisions, and incident energy goes from high to low [26]. In contrast, the dynamical total-proton kurtosis is positive at all incident energies and centralities. Whether the sign change of dynamical net-proton kurtosis indicates the appearance of critical point, or simply caused by non-critical effects, or experimental cuts, are still not clear. A parallel investigation from

*Electronic address: panxuepx@gmail.com

†Electronic address: wuyf@phyh.ccnuc.edu.cn

known conventional models should be helpful.

The paper is organized as follows. In section II, we first derive the statistical parts of the cumulants of three kinds of conserved charges, i.e., net-baryon, net-electric charge and net-strangeness. They turn out to be the same as the baselines derived from HRG model. Then we estimate the contributions of statistical fluctuations to the RHIC published net-proton cumulants in Section III. We find that the incident energy and centrality dependences of net-proton cumulants are dominated by the statistical fluctuations. In section IV, using the generators of the AMPT default, AMPT with string melting [23], and the Ultra Relativistic Quantum Molecular Dynamics (UrQMD) models [27], the dynamical net- and total-proton kurtosis at nine centralities and seven RHIC/BES energies are presented, respectively. They are both positive, in contrary to the observed sign change of dynamical net-proton kurtosis, but in consistent with the observed data of dynamical total-proton kurtosis. Finally, the summary and conclusions are given in section V.

II. STATISTICAL PART OF THE CUMULANTS

As we know the statistical fluctuations of finite number of particles are well presented by Poisson distribution [19]. The possible charges of a baryon, an electric-charged particle, and a strangeness are respectively 1, 1 or 2, and 1, or 2, or 3. We start from the simplest case. Suppose the baryon (N_1^B) and the anti-baryon (N_{-1}^B) numbers both follow Poisson distribution. The probability of net-baryon ($N_B = N_1^B - N_{-1}^B$) is therefore the cross-correlation of two Poisson distributions, i.e.,

$$\begin{aligned} & f(N_B; \langle N_1^B \rangle, \langle N_{-1}^B \rangle) \\ &= \sum_{x=-\infty}^{\infty} f(N_B + x, \langle N_1^B \rangle) f(x, \langle N_{-1}^B \rangle) \\ &= e^{-\langle N_1^B \rangle - \langle N_{-1}^B \rangle} \sum_{x=-\infty}^{\infty} \frac{\langle N_1^B \rangle^{N_B+x} \langle N_{-1}^B \rangle^x}{x! (N_B + x)!} \\ &= e^{-\langle N_1^B \rangle - \langle N_{-1}^B \rangle} (\langle N_1^B \rangle / \langle N_{-1}^B \rangle)^{N_B/2} I_{N_B} (2\sqrt{\langle N_1^B \rangle \langle N_{-1}^B \rangle}). \end{aligned} \quad (1)$$

Where $\langle N_1^B \rangle$ and $\langle N_{-1}^B \rangle$ are means of N_1^B and N_{-1}^B , respectively. $I_{N_B}(z)$ is the modified Bessel function of the first kind. It is a standard Skellam distribution [28], the same as that derived from HRG model [29].

The cumulants of net-baryon (κ_k^B) can be obtained by the cumulant-generating function (CGF),

$$K_B(t; \langle N_1^B \rangle, \langle N_{-1}^B \rangle) = \sum_{k=0}^{\infty} \frac{t^k}{k!} \kappa_k^B. \quad (2)$$

Where $K_B(t; \langle N_1^B \rangle, \langle N_{-1}^B \rangle) = \ln G(e^t; \langle N_1^B \rangle, \langle N_{-1}^B \rangle)$, and $G(t; \langle N_1^B \rangle, \langle N_{-1}^B \rangle)$ is the probability-generating function

(PGF) of Skellam distribution, i.e.,

$$\begin{aligned} & G(t; \langle N_1^B \rangle, \langle N_{-1}^B \rangle) \\ &= \sum_{N_B=0}^{\infty} f(N_B; \langle N_1^B \rangle, \langle N_{-1}^B \rangle) t^{N_B} \\ &= G(t; \langle N_1^B \rangle) G(1/t; \langle N_{-1}^B \rangle) \\ &= e^{-\langle N_1^B \rangle + \langle N_{-1}^B \rangle + \langle N_1^B \rangle t + \langle N_{-1}^B \rangle / t}. \end{aligned} \quad (3)$$

So the even and odd orders of net-baryon cumulants are,

$$\begin{aligned} \kappa_{2k}^B &= \langle N_1^B \rangle + \langle N_{-1}^B \rangle, \\ \kappa_{2k+1}^B &= \langle N_1^B \rangle - \langle N_{-1}^B \rangle. \end{aligned} \quad (4)$$

They are uniquely determined by the means of baryon and anti-baryon numbers.

For electric charged particles, there are four kinds of particles, charge-one particle (N_1^Q) and anti-particle (N_{-1}^Q), and charge-two particle (N_2^Q) and antiparticle (N_{-2}^Q). Suppose the probability of each number of particles is a Poisson distribution. The probability of net-charge of charge-one particles ($N_{1Q} = N_1^Q - N_{-1}^Q$) is again a Skellam distribution, the same as Eq. (1). While, for charge-two particles, the probabilities of charge ($2N_2^Q$) and anti-charges ($2N_{-2}^Q$) are not a Poisson distribution, but

$$f(2N_2^Q; 2\langle N_2^Q \rangle) = \langle N_2^Q \rangle^{N_2^Q} e^{-\langle N_2^Q \rangle} / N_2^Q!, \quad (5)$$

and

$$f(2N_{-2}^Q; 2\langle N_{-2}^Q \rangle) = \langle N_{-2}^Q \rangle^{N_{-2}^Q} e^{-\langle N_{-2}^Q \rangle} / N_{-2}^Q!, \quad (6)$$

respectively. The probability of the net-charge of charge-two particles ($2N_{2Q} = 2N_2^Q - 2N_{-2}^Q$) is their cross-correlation,

$$\begin{aligned} & f(2N_{2Q}; 2\langle N_2^Q \rangle, 2\langle N_{-2}^Q \rangle) \\ &= \sum_{x=-\infty}^{\infty} f(N_{2Q} + x, \langle N_2^Q \rangle) f(x, \langle N_{-2}^Q \rangle) \\ &= e^{-\langle N_2^Q \rangle - \langle N_{-2}^Q \rangle} \sum_{x=-\infty}^{\infty} \frac{\langle N_2^Q \rangle^{N_{2Q}+x} \langle N_{-2}^Q \rangle^x}{x! (N_{2Q} + x)!}. \end{aligned} \quad (7)$$

So, the probability of the net-charge of all charged particles ($N_Q = N_{1Q} + 2N_{2Q}$) is the convolution of the probabilities of the net-charges of charge-one and charge-two particles, i.e.,

$$\begin{aligned} & f(N_Q; \langle N_1^Q \rangle, \langle N_{-1}^Q \rangle, 2\langle N_2^Q \rangle, 2\langle N_{-2}^Q \rangle) \\ &= \sum_{x=-\infty}^{\infty} f(x; \langle N_1^Q \rangle, \langle N_{-1}^Q \rangle) f(N_Q - x; 2\langle N_2^Q \rangle, 2\langle N_{-2}^Q \rangle) \\ &= \sum_{x=-\infty}^{\infty} e^{-\langle N_1^Q \rangle - \langle N_{-1}^Q \rangle} \sum_{n=-\infty}^{\infty} \frac{\langle N_1^Q \rangle^{x+n} \langle N_{-1}^Q \rangle^n}{n! (x+n)!} \\ &\quad \times e^{-\langle N_2^Q \rangle - \langle N_{-2}^Q \rangle} \sum_{m=-\infty}^{\infty} \frac{\langle N_2^Q \rangle^{(N_Q-x)/2+m} \langle N_{-2}^Q \rangle^m}{m! ((N_Q-x)/2+m)!}. \end{aligned} \quad (8)$$

From its CGF and PGF, we can easily get the even and odd orders of net-charge cumulants,

$$\begin{aligned}\kappa_{2k}^Q &= \langle N_1^Q \rangle + \langle N_{-1}^Q \rangle + 2^{2k}(\langle N_2^Q \rangle + \langle N_{-2}^Q \rangle), \\ \kappa_{2k+1}^Q &= \langle N_1^Q \rangle - \langle N_{-1}^Q \rangle + 2^{2k+1}(\langle N_2^Q \rangle - \langle N_{-2}^Q \rangle).\end{aligned}\quad (9)$$

They are also consistent with those obtained from HRG model [29]. It should be noticed that the ratio κ_4^Q/κ_2^Q , i.e., the product of kurtosis and variance, is

$$\frac{\kappa_4^Q}{\kappa_2^Q} = \kappa_4^Q \sigma_Q^2 = \frac{\langle N_1^Q \rangle + \langle N_{-1}^Q \rangle + 16(\langle N_2^Q \rangle + \langle N_{-2}^Q \rangle)}{\langle N_1^Q \rangle + \langle N_{-1}^Q \rangle + 4(\langle N_2^Q \rangle + \langle N_{-2}^Q \rangle)}.\quad (10)$$

It is not an unity, as the case of net-baryon, or net-proton [30], but determined by the means of the numbers of 4 kinds of charged particles.

For strangeness, there are six kinds of particles, i.e., strange one, two and three particles and antiparticles. If the number of each kind of particles is a Poisson distribution, similarly, we can get the even and odd orders of net-strangeness cumulants,

$$\begin{aligned}\kappa_{2k}^S &= \langle N_1^S \rangle + \langle N_{-1}^S \rangle + 2^{2k}(\langle N_2^S \rangle + \langle N_{-2}^S \rangle) \\ &\quad + 3^{2k}(\langle N_3^S \rangle + \langle N_{-3}^S \rangle), \\ \kappa_{2k+1}^S &= \langle N_1^S \rangle - \langle N_{-1}^S \rangle + 2^{2k+1}(\langle N_2^S \rangle - \langle N_{-2}^S \rangle) \\ &\quad + 3^{2k+1}(\langle N_3^S \rangle - \langle N_{-3}^S \rangle).\end{aligned}\quad (11)$$

They are also the same as those obtained from HRG model [29].

So starting from assumption that all kinds of conserved charge particles and antiparticles are produced independently, or follow the Poisson distribution, we get the distributions of three kinds of net-charges, and their cumulants. They turn out to be the same as those baselines obtained from HRG model, where the Boltzmann approximation is implemented and the quantum effects for electric-charged pion are neglected [29]. It shows that the baselines of the cumulants of conserved charges are in fact the fluctuations of independent particle emission, or pure Poisson-liked statistical fluctuations. They are completely determined by the means of particle and anti-particle numbers.

III. STATISTICAL PART OF THE NET-PROTON CUMULANTS AT RHIC

Since the neutron is not detectable in experiments, the proton is argued to be a good approximation of baryon [31]. Replacing the means of baryon and anti-baryon number in Eq. (4) by means of proton ($\langle N_p \rangle$) and anti-proton ($\langle N_{\bar{p}} \rangle$) numbers, we can get the statistical net-proton cumulants. They are the variance,

$$\sigma_{p,stat}^2 = \langle N_p \rangle + \langle N_{\bar{p}} \rangle,\quad (12)$$

the normalized cumulants, i.e., skewness and kurtosis,

$$S_{p,stat} = \frac{\langle N_p \rangle - \langle N_{\bar{p}} \rangle}{(\langle N_p \rangle + \langle N_{\bar{p}} \rangle)^{3/2}}, \quad \kappa_{p,stat} = \frac{1}{\langle N_p \rangle + \langle N_{\bar{p}} \rangle},\quad (13)$$

and the ratios of the third and fourth cumulants to the second one, i.e., the products of skewness and standard deviation, and kurtosis and variance,

$$S_{p,stat} \sigma_{p,stat} = \frac{\langle N_p \rangle - \langle N_{\bar{p}} \rangle}{\langle N_p \rangle + \langle N_{\bar{p}} \rangle}, \quad \kappa_{p,stat} \sigma_{p,stat}^2 = 1.\quad (14)$$

From these expressions, we can see that except $\kappa_{p,stat} \sigma_{p,stat}^2$ is a constant, all others are determined by the means of proton and anti-proton numbers. It is known that with increase of incident energy, and in more central collisions, the means of proton and anti-proton numbers increase, and the relative mean of net-proton (the mean of net-proton divided by the mean of total-proton) decreases. So only the variance, i.e., the width of the net-proton distribution increases with incident energy, and in more central collision. All statistical cumulants decrease with incident energy, in particular, the $S_p \sigma_p$ decreases faster, and the skewness (S_p) is the fastest. This is why all order cumulants are close to each other at the low RHIC/BES energies, where the statistical fluctuations are larger. With increase of incident energies, the third cumulant decreases rapidly and is separated from all other cumulants, cf., the Fig. 1 of ref. [17], and Fig. 2 of ref. [32].

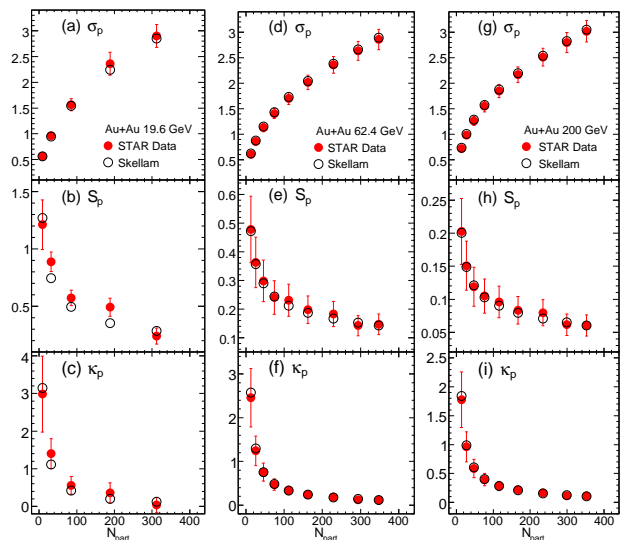


FIG. 1: (Color online) Centrality dependence of the statistical standard deviation (σ_p) (upper row), skewness (S_p) (intermediate row) and kurtosis (κ_p) (down row) of net-proton distribution (open black circles), and corresponding experimental data (solid red circles) for Au+Au collisions at $\sqrt{s_{NN}} = 19.6$ GeV (left column), 62.4 GeV (intermediate column) and 200 GeV (right column).

From the means of proton and anti-proton numbers at nine centralities and three RHIC energies, $\sqrt{s_{NN}} =$

19.6 GeV, 62.4 GeV and 200 GeV [22], we calculate the statistical standard deviation, skewness and kurtosis of net-proton. They are presented by open black circles in three rows of Fig. 1, respectively. Where the solid red circles are the data, and the three columns from left to right correspond to the three incident energies, respectively.

The figure shows that all statistical cumulants (open black circles) are close to corresponding data (solid red circles). The differences between them are one magnitude smaller. So the statistical fluctuations dominate the centrality and energy dependence of net-proton cumulants at RHIC. As expected, the statistical skewness S_p is greatly suppressed when incident energy increases from 19.6 GeV to 200 GeV.

IV. DYNAMICAL NET- AND TOTAL-PROTON KURTOSIS AT RHIC/BES

In order to see the difference between directly measured cumulants and statistical ones, the dynamical cumulants are recommended and defined as [21, 24],

$$\kappa_{p,dyn} = \kappa_p - \kappa_{p,stat}. \quad (15)$$

It measures the correlations between conserved charges. If the particles are produced independently, the dynamical cumulants are zero.

The calculations from lattice QCD have shown that near critical temperature of chiral phase transition, the kurtosis at $\mu_B = 0$ and $m_q = 0$ is positive. It could be negatively divergent near critical point at non-vanishing chemical potential and physical mass [33]. The non-linear σ -model has demonstrated that if the critical point is approached from high temperature side, the dynamical kurtosis will change from negative to positive [8], although the negative values are very small. The calculations of 3-dimensional Ising model show similar critical behaviour [34]. While, the calculations of 3-dimensional $O(4)$ model show that the kurtosis oscillates between positive and negative. So the negative kurtosis is not specific to the critical end point (Ising universality). It may be associated with chiral phase transition ($O(4)$ universality) [14]. Anyway, the behaviour of dynamical kurtosis at RHIC/BES is highly interesting.

The dynamical net- and total-proton kurtosis at nine centralities and seven RHIC/BES energies ($\sqrt{s_{NN}} = 7.7, 11.5, 19.6, 27, 39, 62.4$ and 200 GeV) are shown in Fig. 2(a) and 2(e), respectively [26]. Fig. 2(a) shows clearly how the dynamical net-proton kurtosis varies with two controlling parameters, i.e., incident energy and centrality. It is negative at non-central collisions and higher incident energy, i.e., $\sqrt{s_{NN}} > 19.6$ GeV, and positive at $\sqrt{s_{NN}} < 19.6$ GeV. Where the black solid circles for the most peripheral collisions highlight this change. The positive and negative of dynamical net-proton kurtosis indicate respectively that the peaks of net-proton distributions are sharper and flatter than those of corresponding Skellam distributions.

We can also see from the figure that the values of dynamical kurtosis are not zero, and one magnitude smaller than that directly measured. This indicates that proton and anti-proton are not independently produced at RHIC.

In order to see if this negative kurtosis is caused by non-critical effects, or conventional particle production mechanisms, we calculate the dynamical kurtosis in the AMPT default, the AMPT with string models [23], and the UrQMD model [27], where no critical behaviour is implemented in these models. As we know, the initial size fluctuations are well taken into account in these three transport models by Glaube model. However, the electric charge conservation of produced particles is not fully preserved in the AMPT models. As a compensation, the UrQMD model is better in taking the conservation of final state charges into account.

We simulate Au + Au collisions at seven corresponding incident energies by these three models. The calculations of dynamical net-proton cumulants are performed in the same way as experimental analysis [22]. The centrality bins are selected by the multiplicity of charged particles except proton and anti-proton within pseudo-rapidity window $|\eta| < 0.5$. The proton and anti-proton measurements are carried out at mid-rapidity window $|y| < 0.5$ in the transverse momentum range $0.4 < p_T < 0.8$ GeV/c. The dynamical net- and total-proton kurtosis in each centrality bin are estimated by the centrality bin with correction (CBWC) method [35]. The net- and total-proton kurtosis are presented in the upper and down rows of Fig. 2, respectively. Where the first column is the data from RHIC/STAR. The second, third and fourth columns are the results from the AMPT default, the AMPT with string melting, and the UrQMD models, respectively.

From the upper row of Fig. 2, we can see that the dynamical net-proton kurtosis from three model calculations are all positive at given centralities and incident energies, in contrary to the data in Fig. 2(a). So the conventional particle production mechanisms implemented in three transport models can not reproduce the observed sign change of dynamical net-proton kurtosis. This inconsistency indicates at least that if it is not the transition related behaviour, there should be additional correlations which has not been taken into account in these three transport models.

Whether is it critical related sign change? We have to be very careful in making the conclusion. Since the absolute value of negative kurtosis is very small, less than 0.1, if the experimental cuts, such as the phase space windows of the analysis, the definition of centrality and the centrality bin width corrections [35], the results may change accordingly. But, up to now, how to choose experimental cuts and how to reduce the non-critical effects are still in progressing. So it is not ready yet for a conclusion.

On the other hand, the obtained results from current theoretical calculations and experimental measurements are encouraging. The behaviour of dynamical kurtosis is very interesting, and worthwhile for the further investi-

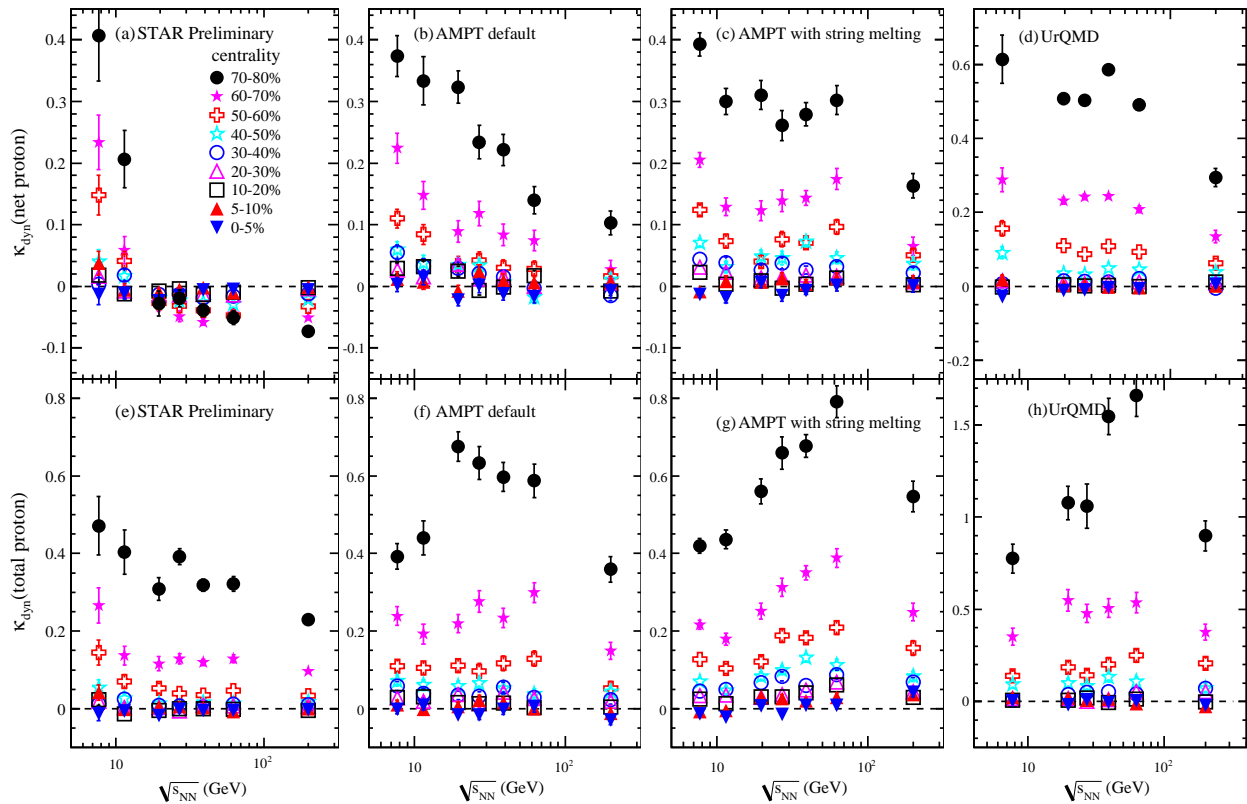


FIG. 2: (Color online) Energy dependence of the dynamical net (upper row), and total (down row) proton kurtosis at nine centralities for Au+Au collisions at RHIC/BES. The results come from experimental data ((a) and (e)) [26], the AMPT default model ((b) and (f)), the AMPT with string melting model ((c) and (g)), and the UrQMD model ((d) and (h)), respectively.

gations.

From the down row of Fig. 2, we can also see that the dynamical total-proton kurtosis from three model calculations are all positive, in consistent with data. They are similar to those of dynamical net-proton kurtosis, shown in upper row of Fig. 2. So there is no significant difference between conserved and non-conserved charge in model calculations. However, the experimental data in Fig. 2(a) and (e) show that the behaviour of conserved charge is quite different from that of non-conserved charge. This indicates again that some correlations between conserved charges are missed in these three transport models.

The quantitative difference between two versions of the AMPT and the UrQMD models lies in peripheral collisions. Where the results from the UrQMD model are all much larger than those from two versions of AMPT model. This may be caused by a strict conservation of final state charged particles in the UrQMD model. It leads to a stronger correlation between charged particles in peripheral collisions, where the number of produced particles are smaller than those of central collisions.

V. SUMMARY AND CONCLUSIONS

In the paper, we argue that at RHIC incident energies, the Poisson-like statistical fluctuations in high cumulants of conserved charges are not negligible. Starting from independent particle production, i.e., assuming the Poisson distribution for the number of conserved charge particles, we derive the statistical cumulants of net-baryon, net-electric charge, and net-strangeness. They are uniquely determined by the means of charged particle and anti-particle numbers, and the same as those baselines obtained from HRG model. So the baselines of higher order cumulants of conserved charges are essentially the statistical fluctuations.

From the means of proton and anti-proton numbers given by RHIC/STAR experiments, we estimate the statistical standard deviation, skewness, and kurtosis. They are close to the data at nine centralities and three RHIC incident energies. So the net-proton cumulants at RHIC are dominated by the statistical fluctuations.

Subtracting the statistical fluctuations, the dynamical

kurtosis of net- and total-proton from two versions of the AMPT and the UrQMD models at RHIC/BES energies are presented. It is found that dynamical net-proton kurtosis is small, but not zero. This indicates that proton and anti-proton are not produced independently in these models, in consistent with data.

However, the observed sign change of dynamical kurtosis of net-proton at RHIC/BES can not be reproduced by conventional particle production mechanisms implemented in these three models. The inconsistency between the model calculations and experimental data indicates at least that if it is not QCD phase transition related behaviour, there should be additional correlations between conserved charges in heavy ion collisions which has not been implemented in these three transport models.

In addition, model calculations show dynamical total-proton kurtosis are all positive at observed centralities and energies, in consistent with data. There is no significant difference between net- and total-proton kurtosis,

or between conserved and non-conserved charges. However, from current experimental data, the centrality and energy dependence of dynamical net-proton kurtosis has a sign change, and the dynamical total-proton kurtosis keeps positive. The behaviour of dynamical net-proton kurtosis is significantly different from that of total-proton kurtosis. It shows again that some correlation effects in conserved charges are missed in these models. So the higher order cumulants provide a more precise examination for the mechanisms of particle production.

VI. ACKNOWLEDGEMENT

This work is supported in part by the NSFC of China with project No. 10835005, 11221504, 11005046, and 11005045, and the MOE of China for doctoral site with project No. 20120144110001.

-
- [1] M. Asakawa and K. Yazaki, Nucl. Phys. A **504**, 668 (1989).
- [2] Z. Fodor and S. D. Katz, Phys. Lett. B **534**, 87 (2002); JHEP 03 (2002) 014.
- [3] C. Schmidt, C. R. Allton, S. Ejiri, S. J. Hands, O. Kaczmarek, F. Karsch, and E. Laermann, Nucl. Phys. B (Proc. Suppl.) **119**, 517 (2003); R. V. Gavai, Nucl. Phys. A **862**, 104 (2011).
- [4] M. Stephanov, K. Rajagopal, and E. Shuryak, Phys. Rev. Lett. **81**, 4816 (1998).
- [5] Y. Hatta and M. A. Stephanov, Phys. Rev. Lett. **91**, 102003 (2003).
- [6] S. Ejiri, F. Karsch, and K. Redlich, Phys. Lett. B **633**, 275 (2006).
- [7] M. A. Stephanov, Phys. Rev. Lett. **102**, 032301 (2009).
- [8] M. A. Stephanov, Phys. Rev. Lett. **107**, 052301 (2011).
- [9] S. Ejiri, F. Karsch, E. Laermann, C. Miao, S. Mukherjee, P. Petreczky, C. Schmidt, W. Soeldner, and W. Unger, Phys. Rev. D **80**, 094505 (2009).
- [10] A. Bazavov *et al.* (HotQCD Collaboration), Phys. Rev. D **85**, 054503 (2012).
- [11] F. Karsch and K. Redlich, Phys. Lett. B **695**, 136 (2011); P. Braun-Munzinger, B. Friman, F. Karsch, K. Redlich, and V. Skokov, Phys. Rev. C **84**, 064911 (2011).
- [12] O. Kaczmarek, F. Karsch, E. Laermann, C. Miao, S. Mukherjee, P. Petreczky, C. Schmidt, W. Soeldner, and W. Unger, Phys. Rev. D **83**, 014504 (2011).
- [13] A. Bazavov *et al.* (HotQCD Collaboration), Phys. Rev. D **86**, 034509 (2012).
- [14] B. Friman, F. Karsch, K. Redlich, and V. Skokov, Eur. Phys. J. C **71**, 1694 (2011).
- [15] S. Mukherjee and M. Wagner, arXiv: 1307.6255.
- [16] A. Bzdak, V. Koch, and V. Skokov, Phys. Rev. C **87**, 014901 (2013).
- [17] Xiaofeng Luo (for the TAR Collaboration), Nucl. Phys. A **904**, 911c (2013).
- [18] A. Bzdak and V. Koch, Phys. Rev. C **86**, 044904 (2012).
- [19] A. Bialas and R. Peschanski, Nucl. Phys. B **273**, 703 (1986); Nucl. Phys. B **308**, 857 (1988); Phys. Lett. B **207**, 59 (1988).
- [20] E. A. De Wolf, I. M. Dremin, and W. Kittel, Phys. Report **270**, 1 (1996); C. Athanasiou, K. Rajagopal, and M. Stephanov, Phys. Rev. D **82**, 074008 (2010).
- [21] C. Pruneau, S. Gavin, and S. Voloshin, Phys. Rev. C **66**, 044904 (2002); J. Adams *et al.* (STAR Collaboration), Phys. Rev. C **68**, 044905 (2003); B. I. Abelev *et al.* (STAR collaboration), Phys. Rev. C **79**, 024906 (2009).
- [22] M. M. Aggarwal *et al.* (STAR Collaboration), Phys. Rev. Lett. **105**, 022302 (2010).
- [23] Z. W. Lin, C. M. Ko, B. A. Li, B. Zhang, and S. Pal, Phys. Rev. C **72**, 064901 (2005).
- [24] Lizhu Chen, Xue Pan, Fengbo Xiong, Lin Li, Na Li, Zhiming Li, Gang Wang, and Yuanfang Wu, J. Phys. G **38**, 115004 (2011).
- [25] V. Skokov, B. Friman, and K. Redlich, Phys. Rev. C **83**, 054904 (2011).
- [26] Zhiming Li (for the STAR Collaboration), Acta. Phy. Polon. B Proc. 6, 445 (2013).
- [27] M. Bleicher *et al.*, J. Phys. G **25**, 1859 (1999).
- [28] J. G. Skellam, Journal of the Royal Statistical Society **109**, 296 (1946).
- [29] P. Braun-Munzinger, B. Friman, F. Karsch, K. Redlich, and V. Skokov, Nucl. Phys. A **880**, 48 (2012).
- [30] Daniel McDonald (for the TAR Collaboration), Nucl. Phys. A **904**, 907c (2013).
- [31] Y. Hatta and M. A. Stephanov, Phys. Rev. Lett. **91**, 102003 (2003).
- [32] L. Adamczyk *et al.* (STAR Collaboration), arXiv: 1309.5681.
- [33] R. V. Gavai and S. Gupta, Phys. Lett. B **696**, 459 (2011).
- [34] Xue Pan, Lizhu Chen, X.S. Chen, and Yuanfang Wu, Nucl. Phys. A **913**, 206 (2013).
- [35] X. Luo (for the STAR Collaboration), J. Phys. Conf. Ser. **316**, 012003 (2011).